High-temperature Steam Oxidation Behavior of Cr-coated Zr Alloy Cladding with Surface Cracks

Youngbeen Yoon, Dongju Kim, Youho Lee *
Seoul National University, 1 Gwanak-ro, Gwanak-gu, Seoul 08826, Korea
**Corresponding author: leeyouho@snu.ac.kr*

***Keywords :** Accident-Tolerant Fuel, Cr coating, cracks, high-temperature steam oxidation, self-healing

1. Introduction

Cr-coated zirconium alloy cladding has been widely investigated as an Accident-Tolerant Fuel (ATF) candidate because the Cr coating can suppress oxidation during normal operation and under high-temperature accident conditions, thereby helping to maintain cladding integrity, particularly the retention of ductility. However, under typical light-water reactor (LWR) operating conditions, chromium is relatively more brittle and less ductile than Zr alloys. Consequently, coating cracks can develop when the cladding experiences local stress/strain concentrations during operation or transients. Once formed, such cracks may serve as preferential pathways for oxygen ingress from the surrounding steam, locally degrading the oxidation-protective performance of the coating. Therefore, oxidation behavior should be assessed not only for intact coating but also for coatings containing cracks.

Numerous studies have reported the high-temperature steam oxidation behavior and protective performance of Cr-coated claddings [1–3], and coating cracking under mechanical loading (e.g., uniaxial tension) has also been reported [4]. In addition, self-healing behavior has been observed in high-temperature steam environments where oxide products fill coating cracks and reduce crack opening. This self-healing behavior potentially restricts oxygen ingress through the crack [5]. Despite these previous studies, quantitative investigations that directly relate oxidation response to measurable crack geometry remain limited. When crack-assisted substrate oxidation competes with crack-filling self-healing, it is necessary to identify the crack-opening regime in which the dominant behavior changes.

Under uniaxial tension, brittle coatings on ductile substrates typically exhibit segmentation cracking in which the surface crack density increases with strain and then approaches a saturation level [3, 6]. Once the crack density saturates (i.e., crack spacing reaches a plateau), further deformation is accommodated mainly by crack opening rather than by formation of new cracks [6]. Accordingly, crack width becomes a direct descriptor of the crack-opening state.

In this work, high-temperature steam oxidation of Cr-coated Zr alloy cladding containing surface cracks is examined, and the conditions under which the coating remains protective are organized using crack width as an observable geometric metric. Surface cracks were introduced by uniaxial tension. Both the short-term and long-term steam oxidation tests were conducted in a thermogravimetric analysis (TGA) under steam; the short-term exposures were designed primarily for post-test characterization of (i) oxide-circle formation beneath cracks and (ii) crack-filling self-healing, whereas the long-term exposure was used to quantify the macroscopic oxidation response by continuously recording time-dependent weight gain, while suppressing inner-surface oxidation. To characterize surface and cross-sectional morphologies and compositions, we used optical microscopy (OM), scanning electron microscopy (SEM), and energy dispersive X-ray spectroscopy (EDS).

2. Experiments

All steam-oxidation tests were performed in a TGA under steam using the same experimental configuration and oxidation protocol as Ref. [1] (including the steam-oxidation setup and the TGA-based weight-gain measurement procedure). In contrast to Ref. [1], where oxidation was performed without mechanical pre-cracking, surface cracks in the present work were intentionally introduced in the Cr coating by uniaxial tension prior to oxidation. Two test campaigns were conducted: short-term exposures for post-test microstructural characterization near cracks, and a long-term exposure for continuous weight-gain measurement while suppressing inner-surface oxidation.

2.1 Short-term steam oxidation tests using dog-bone specimen

Zr-1.1Nb alloy cladding tubes were used as the substrate material. The outer diameter and wall thickness were 9.5 mm and 0.57 mm, respectively. A chromium coating was deposited on the outer surface by arc ion plating (AIP), and three coating thicknesses were examined: 12, 15, and 18 μm.

The coated tubes were machined into dog-bone specimens and strained using an Instron uniaxial testing machine at room temperature (20 °C). The gauge length was 30 mm, and the specimens were strained to 7%, 10%, and 12% (engineering strain) to introduce controlled surface cracks. After tensile pre-cracking, ~1.5 cm-long segments were cut from the gauge length section and used for short-term oxidation tests. The overall workflow is summarized in Fig. 1.

Short-term steam oxidation was conducted in the TGA under steam following the same oxidation protocol as Ref. [1]. Two isothermal exposures were employed: 1200 °C for 10 min and 1100 °C for 30 min. These short exposures were selected to (i) prioritize observation of localized oxidation near cracks (oxide-circle formation and self-healing) and (ii) suppress contributions from oxygen ingress through the inner surface. In particular, the exposure time at 1200 °C was limited to 10 min to minimize inner-surface oxidation. The 1100 °C condition was selected based on Ref. [5], and the 30 min exposure time was determined using a reported correlation for Cr_2O_3 growth kinetics [3] so that the expected oxide scale would be comparable to that formed at 1200 °C for 10 min.

Crack morphology and crack width before oxidation were characterized by top-view SEM. For each condition, 10–20 cracks per specimen were randomly selected, and crack widths were obtained from images taken in the central region of the gauge section (aligned with the tensile axis). Crack widths were quantified via image processing of SEM micrographs. After oxidation, longitudinal cross-sections along the tube axis were prepared, and cross-sectional SEM was used to observe localized oxides formed beneath cracks. The composition of crack-filling products and the oxidation/diffusion behavior near cracks were further examined by SEM/EDS.

Fig. 1. Experimental workflow for short-term steam oxidation tests.

2.2 Long-term steam oxidation test with inner-surface oxidation prevention using Al_2O_3 plugs

The short-term oxidation tests are suitable for observing and quantifying localized oxidation behavior near coating cracks; however, they do not directly capture macroscopic oxidation responses under extended exposure, such as cumulative weight gain and the evolution of coating protectiveness. Therefore, an additional long-term steam oxidation test was performed using a single specimen with relatively large crack openings to minimize the influence of self-healing. The overall procedure and specimen configuration are summarized in Fig. 2.

For the long-term test, the same substrate and coating system described in Section 2.1 were used, and a tubular cladding specimen with a Cr-coating thickness of 20 μm was prepared. Surface cracks were introduced by uniaxial tension at room temperature (20 °C), and an approximately 12 mm-long segment was cut to include the localized deformation region near the fracture. Long-term steam oxidation was then conducted in the TGA under steam following the same oxidation protocol as Ref. [1]. To suppress inner-surface oxidation during the long-term TGA test, the inner flow path was isolated from steam by sealing both ends of the tubular segment with Al_2O_3 plugs (Fig. 2). After the test, cross-sectional SEM/EDS examination confirmed the absence of a ZrO_2 layer on the inner surface (data not shown), indicating that inner-surface oxidation was effectively blocked. Prior to oxidation, crack width and crack spacing were measured by OM, and specimen geometry (e.g., surface area and length) was characterized using a 3D scanner. The crack geometry and specimen dimensions used for the long-term test are summarized in Table I.

Table I: Crack geometry and specimen dimensions of the long-term steam oxidation specimen

Crack width	17–34 μm (mean: 22.56 μm)
Average crack spacing	474 μm
Surface area	311 mm^2
Specimen length	12 mm

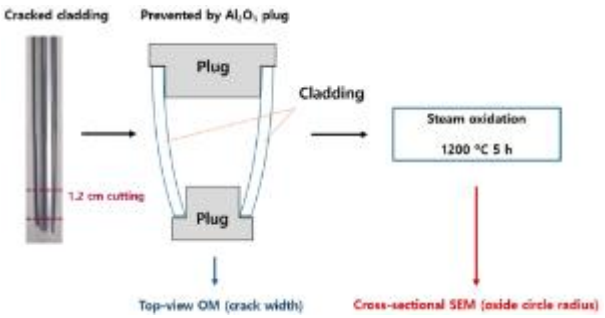

Fig. 2. Long-term steam oxidation experiment setup with inner-surface oxidation prevention using Al_2O_3 plugs.

3. Results and Discussion

3.1 Relationship between crack width and self-healing behavior

In this study, surface cracks were introduced in a controlled manner by applying uniaxial tension to dog-bone specimens to generate tensile cracking in the Cr coating. Top-view SEM observations revealed numerous surface cracks after straining, and Fig. 3(a) shows a representative example. Cross-sectional SEM indicated that most cracks penetrated the coating thickness and terminated at the Cr/Zr interface (Fig. 3(b)). In a few high-strain cases, limited crack-tip

penetration into the substrate was observed. However, cracking and associated damage were largely confined to the Cr coating. This behavior is qualitatively consistent with prior studies on tensile cracking of Cr-coated Zr cladding [4].

Fig. 3(c) shows that crack width increases monotonically with applied strain in the present tensile pre-cracking procedure. Accordingly, the following oxidation and self-healing results are organized using crack width, rather than strain.

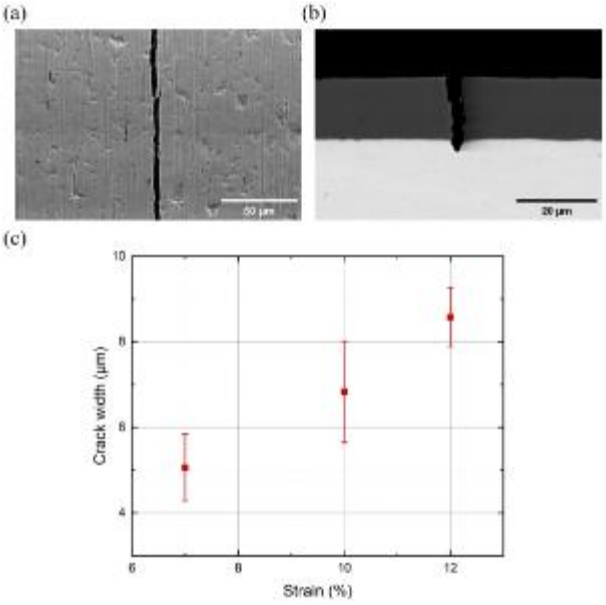

Fig. 3. Controlled tensile pre-cracking (before oxidation): (a) top-view SEM image, (b) cross-sectional SEM image, and (c) crack width as a function of applied strain.

Representative cross-sectional SEM images after steam oxidation show localized substrate oxidation beneath coating cracks, forming a semicircular ZrO_2 region centered beneath the crack (Fig. 4(a, b)). This semicircular oxide region is hereafter referred to as an "oxide circle." During oxide-circle growth, local uplift of the surrounding Cr coating was observed, consistent with the volume expansion associated with the transformation of Zr to ZrO_2 (Pilling-Bedworth ratio, PBR ≈ 1.56). Taken together, these observations are consistent with the interpretation that an open coating crack provides a preferential route for oxygen ingress from the external steam environment to the Zr substrate, thereby promoting crack-assisted localized oxidation.

A thin oxide layer was also observed along the crack sidewalls, formed as Cr_2O_3 through oxidation of the Cr coating (Fig. 4(a, b)). The oxide layer tended to appear thinner near the Cr/Zr interface (arrows in Fig. 4(a, b)). Possible contributors include local oxygen consumption associated with adjacent ZrO_2 growth and/or interfacial redox effects, although further analysis is required.

To quantify the size of the oxide circle, we defined an oxide radius as follows. As illustrated in Fig. 4(c), three radii were measured in cross-section with respect to the crack centerline—left, center, and right—and the oxide radius was defined as the average of these three values. With this definition in place, we subsequently establish the relationship between crack width and oxide radius.

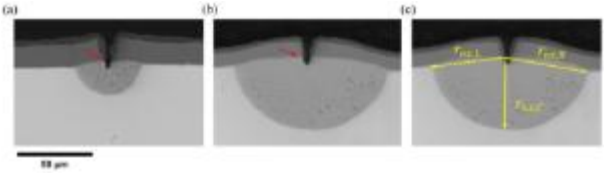

Fig. 4. Cross-sectional SEM images showing oxide-circle formation beneath coating cracks after short-term steam oxidation: (a) 1100 °C–30 min, (b) 1200 °C–10 min, and (c) schematic definition of three directional radii measured beneath a crack.

Oxide-circle formation was not observed beneath every crack. In a subset of cracks, the opening was partially or completely filled with oxidation products, leaving little open gap; this behavior is referred to here as self-healing (Fig. 5). SEM/EDS mapping of such cracks revealed two representative types of crack filling. In some cases, the crack interior was enriched in Cr together with O, consistent with Cr_2O_3-based filling (Fig. 5(a–d)). In other cases, the crack interior exhibited pronounced Zr enrichment (Fig. 5(e–h)). For these Zr-enriched fillings, the corresponding O map does not show a visually distinct increase confined to the narrow crack relative to the surrounding oxide/nearby regions. Thus, the present EDS maps alone are insufficient to uniquely determine the phase identity of the Zr-rich filling (e.g., to confirm ZrO_2). Prior work on Cr-coated Zr-alloy cladding in high-temperature steam has reported crack filling that was attributed to ZrO_2 formation associated with substrate oxidation [5]. In light of this literature context, the Zr enrichment observed here is considered consistent with a Zr-based oxide filling mechanism, although direct phase confirmation is not available in the present dataset. Notably, the Zr substrate beneath oxide-filled cracks typically showed only a very small oxide circle or none at all, which suggests that once the crack opening becomes filled, oxygen ingress through that crack may be reduced.

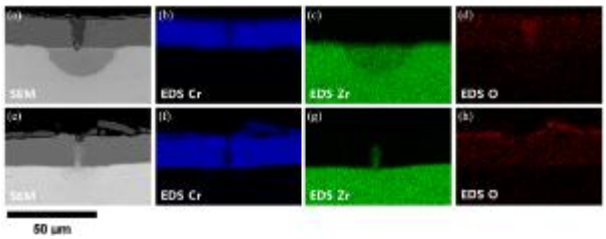

Fig. 5. SEM images and corresponding EDS maps of crack-filling products after short-term steam oxidation, showing (a–d) Cr_2O_3-based healing and (e–h) Zr-rich healing products.

To examine the effect of crack opening on localized substrate oxidation, the oxide radius was plotted against crack width for individual cracks, grouped by coating thickness (12, 15, and 18 μm) and oxidation condition (1100 °C–30 min and 1200 °C–10 min) (Fig. 6). For small crack widths, oxide radii were near zero or only a few micrometers. With increasing crack width, oxide radii generally increased to the order of several tens of micrometers. This transition-like branching behavior is consistent with the interpretation that sufficiently open cracks can sustain oxygen access to the substrate and promote crack-driven oxidation, whereas narrow cracks tend to suppress localized oxidation because the opening is reduced by crack filling and/or oxygen supply within the crack becomes limited.

For the purpose of organizing the dataset, Fig. 6 highlights a visually selected operational transition range (shaded band) around ~5–6 μm crack width. This shaded band is intended only as a guide-to-the-eye indicating where the branching behavior becomes apparent in the present dataset; it should not be interpreted as a mechanistically derived or well-defined physical threshold. Above this operational transition range, oxide radii remain scattered. Such scatter likely reflects variations in local opening geometry and crack path, differences in the surrounding microstructure, and locally occurring oxide growth, spallation, or partial crack filling. In this dataset, the scatter in the larger-opening regime appears more pronounced at 1100 °C than at 1200 °C. One plausible contributor is that the short-term exposure times were selected so that expected Cr_2O_3 growth would be comparable between 1100 °C–30 min and 1200 °C–10 min, whereas localized substrate oxidation beneath cracks may not scale identically with this time adjustment. Quantitatively identifying the origin of this temperature-dependent difference is beyond the scope of this work and requires additional investigation.

To present self-healing more clearly, Fig. 7 plots crack width as a function of Cr-coating thickness and classifies each crack into two operational categories based on oxide radius: cracks with an oxide radius ≥ 10 μm are labeled as “unhealed,” whereas those with a radius < 10 μm are labeled as “self-healed.” This cutoff is introduced solely for consistent visualization and does not represent a mechanistic threshold.

Under the 1100 °C–30 min condition (Fig. 7(a)), the two groups exhibit only modest variation with coating thickness, and the scatter in the data prevents drawing conclusions about any thickness-dependent trend. Under the 1200 °C–10 min condition (Fig. 7(b)), no clear thickness dependence is observed, and the transition-like branching appears around a crack-width range of ~5–6 μm. Overall, self-healing is predominantly associated with smaller crack openings within this operational framework.

In summary, under the present short-term oxidation conditions, localized substrate oxidation induced by coating cracks (oxide-circle formation) is primarily governed by crack width. Below a certain crack width, the oxide radius remains limited due to self-healing and restricted oxygen ingress. Above that range, oxygen ingress is sustained and the oxide radius increases significantly, showing a transition-like (branching) behavior around the operational transition range (~5–6 μm). Based on this observation, the long-term oxidation test in Section 3.2 employed a specimen with crack widths well above the operational critical crack width (~5–6 μm) to minimize the influence of self-healing and to examine the macroscopic impact of crack-driven oxidation.

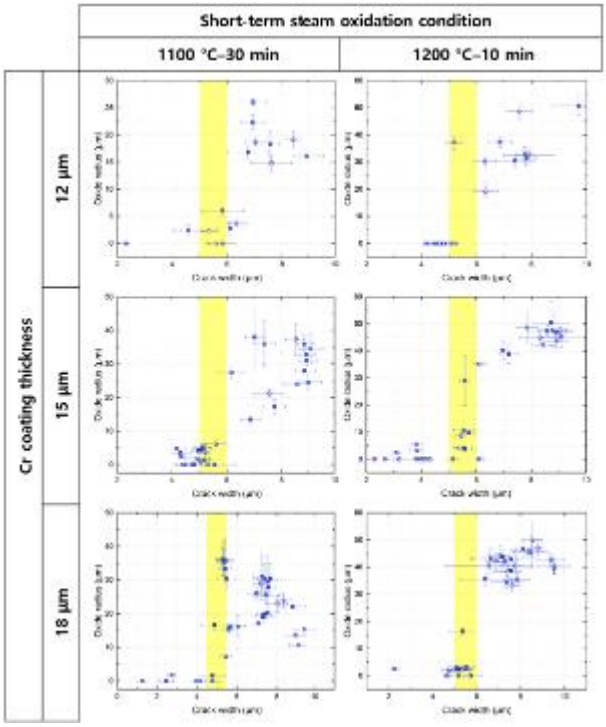

Fig. 6. Correlation between crack width and oxide radius measured after short-term steam oxidation. The six panels are arranged as a 2×3 grid by oxidation condition (columns: 1100 °C–30 min and 1200 °C–10 min) and Cr coating thickness (rows: 12, 15, and 18 μm).

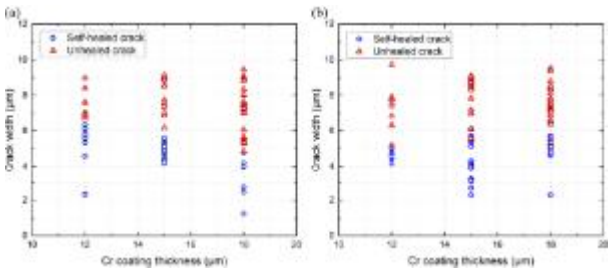

Fig. 7. Classification of self-healed and unhealed cracks as a function of Cr coating thickness and crack width after short-term steam oxidation at (a) 1100 °C for 30 min and (b) 1200 °C for 10 min.

The self-healing behavior characterized in this study was observed exclusively under isothermal high-

temperature oxidation conditions (1100°C–30 min and 1200°C–10 min) and may not directly translate to the non-isothermal transients representative of an actual loss-of-coolant accident (LOCA) scenario, where sustained high-temperature oxidation is followed by rapid quenching upon actuation of emergency core cooling. During quenching, thermal stresses arise at the interfaces due to the coefficient of thermal expansion (CTE) mismatch among the Zr substrate, Cr coating, and the thermally grown oxides (Cr_2O_3 and ZrO_2). Critically, the regions adjacent to self-healed cracks are characterized by a compositionally and structurally heterogeneous cross-section—comprising crack-filling oxide products (Cr_2O_3-based or Zr-rich filling), residual Cr coating, and the underlying Zr substrate—in contrast to the relatively homogeneous layered structure of neighboring intact-coating regions. This local compositional inhomogeneity may give rise to non-uniform thermal stress distributions during rapid cooling, potentially rendering healed crack regions more susceptible to interfacial decohesion or re-cracking under thermal shock than the surrounding intact coating. Accordingly, the protective role of self-healing identified in this work is strictly applicable to the isothermal oxidation phase, and its persistence through the subsequent quenching transient—a critical element of accident progression—remains uncharacterized and warrants dedicated experimental investigation.

3.2 Long-term oxidation behavior of Cr-coated Zr alloy cladding containing cracks

This section presents the results of a long-term steam oxidation test (1200 °C for 5 h) performed on a specimen containing surface cracks with widths sufficiently larger than the operational critical crack width (~5–6 μm) identified from the short-term tests. Inner-surface oxidation was blocked using Al_2O_3 plugs. The long-term specimen geometry (crack width, crack spacing, etc.) was intentionally selected to minimize the influence of self-healing, as summarized in Table I. Because this long-term dataset is based on a single pre-cracked specimen (n = 1) and does not include an intact control specimen under the same condition, the comparisons below are presented qualitatively using a literature-based intact baseline.

Fig. 8(a) shows the specimen weight gain (WG) as a function of time during long-term oxidation. WG increases steadily over 0–300 min, exhibiting mild curvature in the early stage but becoming nearly linear thereafter. Fig. 8(b) plots the corresponding WG rate (dWG/dt). After a brief start-up transient, a relatively high WG rate is reached within ~10–20 min and then decreases. After ~100 min, the WG rate remains nearly constant at ~0.33–0.35 mg/min.

Previous long-term oxidation studies on intact Cr-coated cladding have reported a “transition” behavior: the coating initially maintains protectiveness, and after a certain time the oxidation rate increases (i.e., loss of protectiveness). When the literature model is applied [2], the predicted time to loss of protectiveness for a 20 μm coating is ~200 min.

By contrast, the present pre-cracked specimen shows no clear low-rate incubation period. Instead, the WG rate is comparatively high from the early stage and remains elevated thereafter. This qualitative difference suggests that, when cracks are present, oxidation akin to a loss-of-protectiveness regime may occur from the outset. We note, however, that the present long-term dataset is limited to a single specimen (n = 1) without an intact control under the same condition. Post-test cross-sectional SEM/EDS confirmed that no ZrO_2 scale formed on the inner surface (data not shown), supporting that the long-term weight-gain response is not affected by inner-surface oxidation.

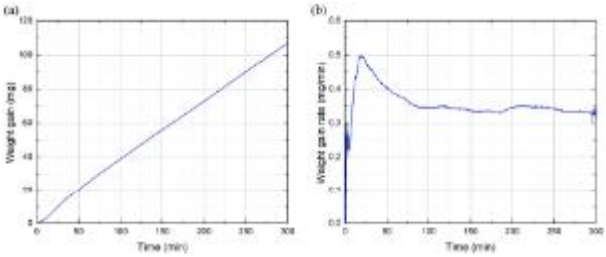

Fig. 8. TGA-measured weight gain response of the long-term steam oxidation specimen during 1200 °C–5 h with inner-surface oxidation prevented: (a) weight gain vs time, (b) weight gain rate vs time.

Cross-sectional SEM images and the corresponding Zr EDS maps obtained after the 1200 °C–5 h steam exposure are summarized in Fig. 9. In regions where the Cr coating remained continuous (Fig. 9(a, b)), the Zr signal appeared intermittently along Cr grain boundaries and near the Cr/Zr interface. Such localized Zr enrichment is consistent with the formation of short-circuit transport features within the coating [1]. However, within the present observations, these features did not develop into a visually continuous ZrO_2 layer extending beneath the coating. At the scale examined here, the intact-coating regions therefore show limited evidence of through-coating substrate oxidation compared with the crack-affected locations.

In contrast, sections taken at surface cracks (Fig. 9(c, d)) reveal a markedly thicker and more developed ZrO_2 region beneath the crack opening, consistent with crack-assisted access of oxidant to the substrate. Notably, the crack-adjacent ZrO_2 frequently contained large cavities/porosity, and similar voided morphologies were observed at multiple crack sites. Although the origin of this porosity was not resolved in the present work, its repeated occurrence indicates that the oxide formed under crack-fed conditions can differ morphologically from oxides associated with intact coating regions, which may in turn influence local transport and oxidation progression.

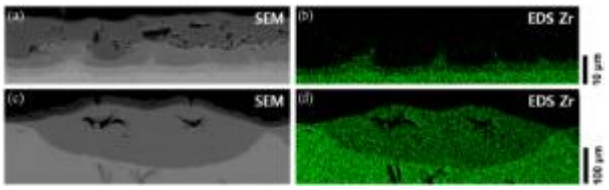

Fig. 9. Cross-sectional SEM images and corresponding Zr EDS maps of the specimen after steam oxidation at 1200 °C for 5 h: (a) SEM image of an intact coating region, (b) Zr EDS map, (c) SEM image near a surface crack, and (d) Zr EDS map.

To assess whether the macroscopic TGA response can be rationalized by the geometric fraction of substrate directly opened by cracks, an area-fraction estimate was constructed for WG(t) and dWG/dt, and the results are compared with the measurement in Fig. 10. The crack-exposed fraction of the outer surface was approximated from the long-term specimen geometry (Table I) using the mean crack width and average crack spacing, i.e., $\overline{w}/\overline{s}$ = 22.56 μm / 474 μm ≈ 0.0476 (≈ 4.76% of the outer surface). The total weight gain was then represented as the sum of (i) an intact-coating contribution following literature kinetics for Cr-coated cladding (including transition behavior) [1–3] and (ii) an exposed-substrate contribution represented by diffusion-controlled oxidation of bare Zr [7].

This simple decomposition reproduces the qualitative "intact-coating" trend—namely, a delayed increase in WG rate near the expected transition time for a 20 μm coating (≈ 200 min in the cited framework). In the present cracked specimen, however, the WG rate is comparatively high from the early stage and remains elevated rather than exhibiting a clear low-rate incubation period. The deviation indicates that the impact of cracks is not captured by scaling bare-Zr oxidation solely by the geometric opening fraction. A key implication is that crack-fed oxidation can spread sideways beneath the neighboring coating, giving it a reaction footprint larger than the crack itself. The crack region can also experience local changes—such as coating uplift, partial debonding, and the formation of porous or voided oxides—which further modify transport beyond what an area-only estimate would predict. Consequently, Fig. 10 is used here as an order-of-magnitude benchmark to highlight the observed acceleration, rather than as a predictive model for the long-term oxidation kinetics of cracked coatings.

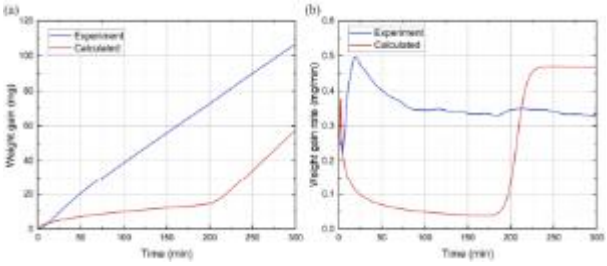

Fig. 10. Comparison between measured and estimated weight gain response for the long-term oxidation test: (a) weight gain vs time, (b) weight gain rate vs time.

4. Conclusion

This study experimentally investigated the high-temperature steam oxidation behavior of Cr-coated Zr-1.1Nb cladding containing surface cracks. The influence of cracks on coating protectiveness was organized using crack width as the key quantitative metric. Coating cracks were introduced by uniaxial tension, followed by short-term steam oxidation (1100 °C–30 min and 1200 °C–10 min) and long-term steam oxidation (1200 °C–5 h) with inner-surface oxidation prevented using Al_2O_3 plugs.

In the short-term tests, coating cracks acted as oxygen ingress paths, leading to localized oxidation of the underlying Zr substrate and formation of an oxide circle beneath the crack. In parallel, self-healing was observed, where the crack interior became filled with oxidation products and crack opening decreased. For cracks exhibiting self-healing, oxygen ingress through the crack was restricted and the oxide circle tended to be small or absent.

Correlating crack width with oxide radius in the short-term tests revealed transition-like behavior: oxide radius remained limited at small crack width, whereas it increased markedly as crack width increased. To distinguish these regimes, this work introduced an operational critical crack width as a working criterion, and the branching behavior under the present conditions tended to occur around ~5–6 μm. (The operational critical crack width and healed/unhealed classification are operational criteria for organizing the observations. Identifying a strict physical threshold requires further study.)

In the long-term test (1200 °C–5 h), the specimen with cracks well above the operational critical crack width showed continuously increasing WG. Unlike intact coatings, which typically exhibit a low initial WG rate, the cracked specimen displayed a comparatively high rate from the early stage, and this elevated rate persisted throughout the test. Cross-sectional observations showed two distinct behaviors. In intact coating regions, Zr penetration or oxidation appeared mainly along grain boundaries. In contrast, near cracks, the ZrO_2 was more extensively developed and often contained internal voids—features consistent with

crack-driven oxidation that contributes to the long-term WG increase.

Overall, when cracks exist in the Cr coating, they can serve as pathways that induce localized substrate oxidation in high-temperature steam. When crack width is maintained above a certain level, oxide radius tends to grow substantially. These findings indicate that oxidation resistance of Cr-coated cladding should be discussed not only in terms of crack presence, but also in terms of crack width. Future work should (i) quantify the operational critical crack width and classification criteria (including uncertainty), (ii) elucidate the mechanisms of self-healing/oxide formation and the origin of void formation, and (iii) develop quantitative models incorporating the 2D (radial) diffusion field and deformation-microstructure effects near cracks to quantitatively separate the contribution of crack-induced oxidation, (iv) evaluate the structural integrity of self-healed crack regions under thermal shock conditions representative of LOCA quenching, where CTE-mismatch-induced stresses may compromise the protective function of the healing products.

Acknowledgement

This work was supported by the Korea Institute of Energy Technology Evaluation and Planning(KETEP) and the Ministry of Climate, Energy & Environment(MCEE) of the Republic of Korea (No. RS-2022-KP002856).

REFERENCES

[1] D. Kim and Y. Lee, Mechanisms of Steam Oxidation-Induced Degradation of Chromium Coating on Zirconium Alloys at High Temperatures, Corrosion Science, Vol. 254, p. 113055, 2025.
[2] D. Kim and Y. Lee, An integral mechanistic model for the degradation and protection loss of Cr-coated zirconium alloys in steam oxidation environments, Corrosion Science, Vol. 260, p. 113565, 2026.
[3] H. Kang, D. Kim, S. Martin, and Y. Lee, Parabolic oxidation for various chromium-coated Zr-Nb Alloy Claddings, Journal of Nuclear Materials, Vol. 615, p. 155946, 2025.
[4] J. Jiang, D. Zhan, J. Lv, X. Ma, X. He, D. Wang, Y. Hu, H. Zhai, J. Tu, W. Zhang, and B. Wang, Comparative study on the tensile cracking behavior of CrN and Cr coatings for accident-tolerant fuel claddings, Surface & Coatings Technology, Vol. 409, p. 126812, 2021.
[5] H. B. Ma, Y. H. Zhao, Y. Liu, J. T. Zhu, J. Yan, T. Liu, Q. S. Ren, Y. H. Liao, G. Liu, X. D. Lin, and M. Y. Yao, Self-healing behavior of Cr-coated Zr alloy cladding in high temperature steam oxidation process, Journal of Nuclear Materials, Vol. 558, p. 153327, 2022.
[6] A. P. McGuigan, G. A. D. Briggs, V. M. Burlakov, M. Yanaka, and Y. Tsukahara, An elastic–plastic shear lag model for fracture of layered coatings, Thin Solid Films, Vol. 424, No. 2, pp. 219-223, 2003.
[7] D. Kim, H. Yook, K. Keum, and Y. Lee, TRANOX: Model for Non-isothermal Steam Oxidation of Zircaloy Cladding, Journal of Nuclear Materials, Vol. 556, p. 153153, 2021.